Conference on Modelling Fluid Flow (CMFF'22)
The 18th International Conference on Fluid Flow Technologies
Budapest, Hungary, August 30 -September 2, 2022

FLOW AROUND BUBBLES: 4D MEASUREMENT CONCEPT WITH HIGH-SPEED TOMOGRAPHIC SYSTEM

C. Müller[1*], Y. Chang[1,2], P. Kováts[1], D. Thévenin[1], K. Zähringer[1]

[1] Laboratory of Fluid Dynamics and Technical Flows, Otto-von-Guericke-Universität Magdeburg. Universitätsplatz 2, D-39106 Magdeburg, Germany. Tel.: +49 391 - 67 58654, Fax: +49 391 - 67 52840
[2] State Key Laboratory of Multiphase Flow in Power Engineering, Xi'an Jiaotong University, Xi'an 710049, China
*E-mail: conrad.mueller@ovgu.de

ABSTRACT

The motion and form of single bubbles are investigated usually with 2D optical measurement methods, like shadow imaging or Particle Image Velocimetry (PIV) [1-3]. With improving optical measurement techniques and image processing it becomes possible to investigate single bubbles or bubble groups in a 3D volume with tomographic measurement techniques.

In the present study, small bubble groups and the liquid flow around them are investigated in a stagnant liquid with 4D shadow imaging and 4D particle tracking. Applying four high-speed cameras and LED volume illumination, images of the bubbles and tracer particles are recorded simultaneously. During image processing, bubbles and particles are treated separately. The bubbles are reconstructed with the help of a tomographic sizing algorithm and the centre of mass of the reconstructed 4D objects is tracked, what results in 4D bubble trajectories. From these measurements not only the 3D bubble path and bubble velocity, but also the bubble size, shape and its deformation can be obtained.

Additionally, the segmented tracer particles are used to calculate the instantaneous 3D liquid flow field around the bubble groups with the Shake-the-box algorithm, which is a 4D particle tracking velocimetry method.

This kind of experiments delivers data for the modelling of bubble dynamics in gas-liquid contactors, as e.g. bubble columns, and can be a good validation base for 3D CFD simulations with single bubbles and interactions between multiple bubbles in a bubble swarm.

Keywords: PTV, Shadow imaging, Shake-the-box, Tomographic sizing, Trajectories, Two-phase flow

1. INTRODUCTION

Investigations on single bubbles in two-phase flows, their motion, interactions with each other and with the surrounding liquid is important for the deeper understanding of mass transfer in these systems. Especially for the scale-up process of bubble columns these data are important. Also the validation of numerical simulations demand experimental data with high spatial and temporal resolution. Comparable measurements, e.g. by Hassan et. al., Liu et al. or Yoshimoto et al. [4-6], have been carried out for single bubbles, nevertheless for only the bubble motion, only the liquid flow field or in low temporal resolution.

Recently modern three-dimensional measuring techniques are highly improving in terms of spatial and temporal resolution and optical accessibility. The range of different measurement methods to characterize a flow field and their processing ranges from tomographic PIV, over PTV to high resolution time-resolved PTV, using modern processing algorithms like Shake-the-Box (STB) [7]. This enables tomographic high-speed measurement systems with PTV to increase the spatial resolution, because the algorithm can handle higher particle concentrations than common PTV algorithms. For the postprocessing the Fine Scale Reconstruction (FSR) algorithm introduced by Schneiders et al. 2018 [8] is used. All those measurement systems have been compared and their capabilities tested e.g. by Sellappan et. al. 2020 [9] for single phase jet flows. Even combinations of flow velocity measurements using high-speed PIV or tomographic PIV with shadow imaging were performed by Lee and Park 2022 [10] or She et al. 2021 [11]. All these methods are only applicable for low gas contents otherwise single bubbles cannot be recognized nor be reconstructed. Neither can the flow be measured, due to illumination purposes.

In order to investigate the bubble motion of multiple bubbles in a bubble swarm together with the flow field around the bubbles, in this study high-speed shadow imaging is used. By segmenting the bubble shadows from those of tracer particles in the surrounding water, the bubble motion, size and shape can be tracked and reconstructed. The tracer particle field is then used to calculate the flow field in the investigated volume.

The results from such measurements can be used as validation for bubble interaction simulations such as performed by Zhang et al. [12,13].

NOMENCLATURE

d_{eq}	[mm]	bubble equivalent diameter
Q	[-]	Q-criterion
t	[ms]	time (step)
v_B	[m/s]	bubble velocity
v_L	[m/s]	liquid velocity

2. EXPERIMENTAL SETUP

For the tomographic setup a decagonal acrylic glass tank with a gas inlet in the centre of the bottom was filled with de-ionised water. Four Phantom VEO L640 high-speed cameras (2560x1600 pixels) were set along a horizontal line in an arc-like configuration around the tank, so all camera lenses (Tokina 100 mm) were parallel and equidistant to one face of the tank as shown in Figure 1.

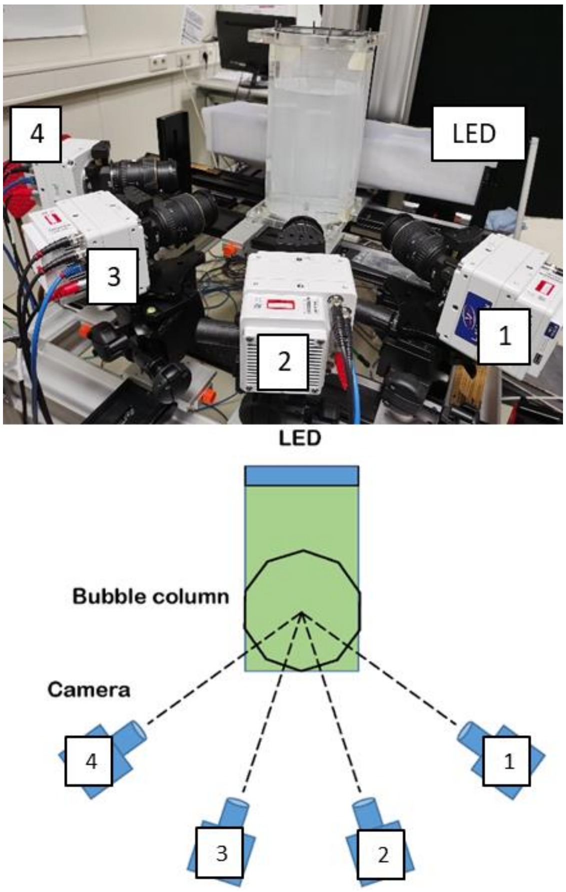

Figure 1. Experimental setup of the four horizontally aligned cameras and the decagonal acrylic glass bubble column with background illumination (top); camera configuration (bottom).

In order to fulfil the Scheimpflug condition all camera's focal planes were aligned with a calibration plate (LaVision 058-5), which was put in the centre of the tank. For the background illumination a triggered blue LED Flashlight 300 (LaVision) and a diffusor were used. For each measurement 5000 images were taken as time-resolved single frames simultaneously with all four cameras at a constant recording frequency of 1 kHz. White Vestosint particles with a mean diameter of 40 µm were used as tracer particles for the liquid phase. The particle concentration was calculated to be 0.0066 ppp (particle per pixel). The images are recorded and mainly processed with DaVis 10.2 (LaVision).

2.1. Calibration

Geometrical calibration, which is a crucial step for the quality of the tomographic reconstruction, has been performed in a two-step procedure: initial geometrical calibration followed by correction with disparity of triangulated particles. For the initial geometrical calibration, a 3D calibration plate (LaVision 058-5) was set first in the centre of the tank and then at two additional positions 5 mm before and 5 mm behind the centre plane. The final calibration reached a fit error of 0.004 pixel with a scale factor of 39.25 pixel/mm for a 1964x2703 pixels dewarped image. The angle between the cameras furthest away from each other (1-4) was 99.53°. The following self-calibration results in an average disparity of 0.03 voxel with a maximum of 0.06 voxel. The final reconstructed volume of 50x68x20 mm³ results in 1963x2702x785 voxels.

For the bubble reconstruction, this original calibration was also scaled down from 39.25 pixel/mm to 25, 12.5 and 6.25 pixel/mm, in order to test the minimization of computing time and final file size (see section 3.2 and 3.3). The influence of the different resolutions on the bubble reconstruction and the trajectories was tested as shown later.

2.2. Flow Conditions

The gas inlet stainless steel capillary had a diameter of 0.13 mm, producing small bubbles, and 1 mm, producing bigger bubbles. Air was introduced by a syringe pump. The investigated rising bubbles can be classified into 5 groups. Single bubbles of different sizes, small bubbles being almost perfectly round with an average diameter of 1 mm, medium bubbles with a diameter of 4 mm and oblate spheroid shape and large bubbles with an instable surface and shape like a jellyfish, which is oscillating. In addition, bubble swarms were measured, with 6-12 medium sized bubbles and one case with very large bubbles with a complex and varying shape. The bubble swarms were produced with manual short and fast pumps (~10 mL) of the syringe without capillary. In both swarms, bubble collisions took place. The gas volume fraction in the measuring volume was always lower than 0.5%.

3. POSTPROCESSING

Most postprocessing procedures are evaluated by the help of DaVis 10.2 from LaVision. The general processing steps and their results are shown in the flow chart in Figure 2.

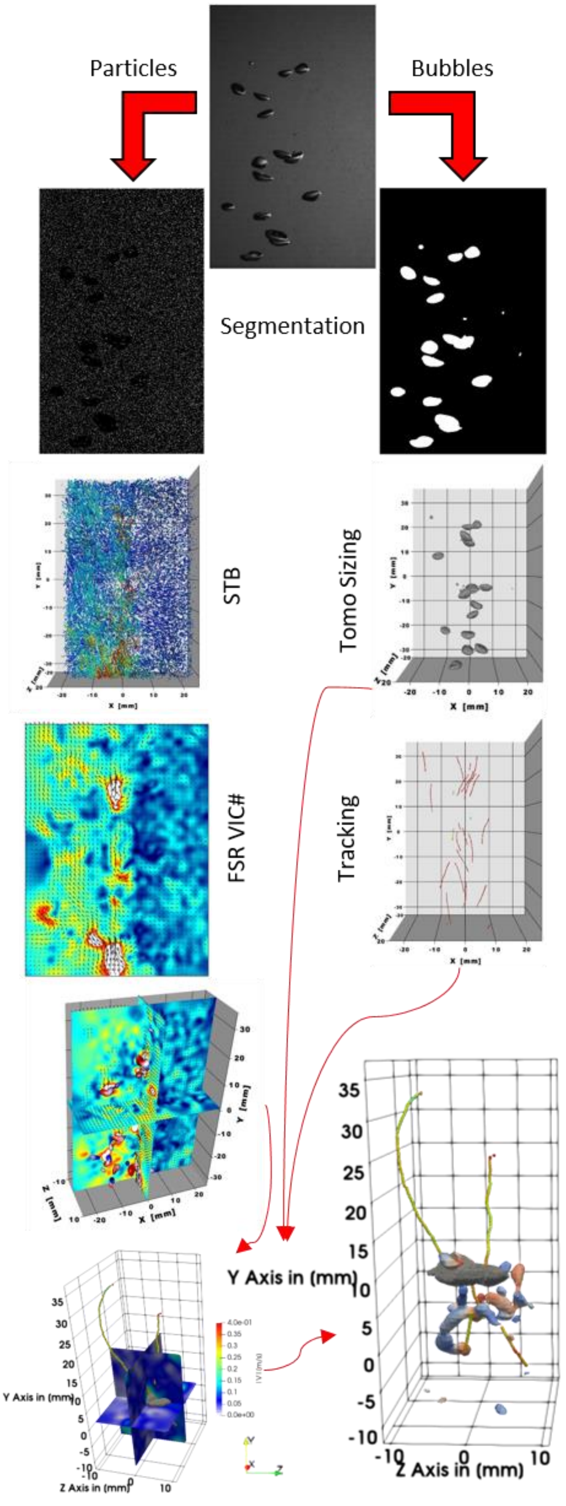

Figure 2. Data postprocessing workflow of the time-resolved shadow imaging measurements.

In the first processing step the tracer particles were separated from the bubble shadows with a segmentation filter and were then treated separately. In the case of bubble swarms with strong differences between large and small bubbles, the small and large bubbles were additionally separated from each other.

For the liquid phase the singled-out particles were reconstructed in 3D and their trajectories were created using the Shake-The-Box algorithm (STB) implemented in DaVis 10.2, which allowed a triangulation error of 1.5 voxel and went for 4 iterations over the inner and outer loop. Particle positions were shaken by 0.1 voxel and have been removed, if being closer than 1 voxel to each other or had a weaker intensity than 0.1 of the average intensity. A minimum required track length of 4 time steps was set with a maximum allowed absolute change in particle shift of 1 voxel and a relative change of 20%. In the next step a time-resolved three-dimensional reconstruction of the flow field was calculated with DaVis 10.2 from the obtained particle trajectories using a fine scale reconstruction (FSR) based on the vector in cell algorithm (VIC#) [14].

For the gas phase, the bubbles were reconstructed using the three-dimensional Tomographic Sizing algorithm implemented in DaVis 10.2. The bubble diameter was calculated from the reconstructed volume of each segment. Segmentation and tracking were then used to determine the centre of gravity of the bubbles and reconstruct the trajectories and bubble rising paths. Velocity, acceleration as well as the bubble equivalent diameter for each time step can then be obtained for all three coordinate directions.

The 3D reconstructions of the bubbles and the volumetric flow field from the FSR VIC+ were then merged with the bubble trajectories in ParaView 5.10. The vorticity and the Q-criterion were also calculated from the flow field.

3.1. Fine Scale Reconstruction VIC#

Since the FSR interpolates the space between the particle trajectories with time-resolved velocity data, the link between the number of trajectories, (thus the found and reconstructed particles from the STB,) and the quality of the FSR is obvious. From 35,000 reconstructed particles in the STB results a particle concentration of 0.0066 ppp. This particle concentration is on the low end of recommended values [15]. As shown in Figure 3 the coarser grids of 24 voxel to 12 voxel show a good agreement of the general vortex structures around the bubbles, but the finest grid of 6 voxel, and so 8 times more vectors than the 12 voxel grid, shows a lot of numerical noise because too much vectors were interpolated between the trajectories, even though the large vortex structures stay in place. In order to use such a fine grid, a higher particle concentration close to 0.125 ppp is recommended. However, higher particle concentrations are only achievable in small volumes avoiding the effect of particles in front and behind the actually measured volume. Particles outside the investigated volume decrease the overall illumination intensity (background-particle intensity ratio) and also blur the recognized particles. Both issues lead to a more inaccurate and worse particle reconstruction.

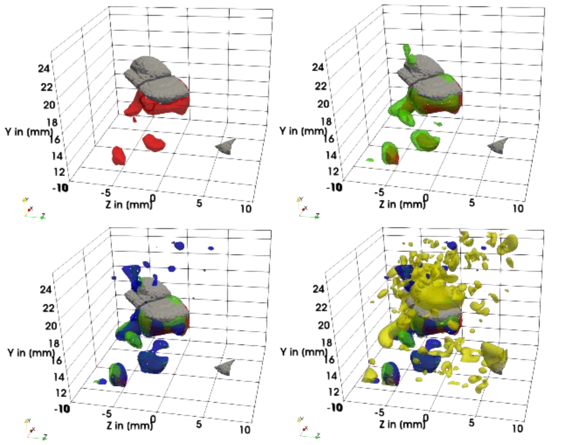

Figure 3. Comparison of vortex structures around two touching bubbles for different grid sizes of Fine Scale Reconstruction VIC#, from top left to bottom right: 24 (red), 16 (green), 12 (blue), 6 (yellow) voxel grid; bubbles in grey.

3.2. Effect of the resolution

The initial resolution of 39.25 pixel/mm was a considerable problem for the reconstruction of the bubbles, due to the large amount of computing power, which requires a very fast CPU and a strong GPU. For loading final images of the reconstruction even a humongous working memory (RAM) is necessary. In order to reduce the computing costs, the resolution of the reconstructions was reduced by downscaling the calibration to 25, 12.5 and 6.25 pixel/mm. The images in Figure 4 show a small, medium and a big bubble as 2D projections of the 3D reconstruction for the different resolutions. It is obvious, that the bigger the bubble, the less the resolution effects the overall reconstructed volume. Nevertheless, for small spherical bubbles the difference of calculated equivalent diameter between low and high resolution is less affected than for big, irregular bubbles. But, it only differs in a negligible range of maximum 0.6%. For later images and calculations, only the lowest resolution of 6.25 pixel/mm was applied for representing the bubbles and the trajectories to minimize computing time. It has to be noted, that even for very high resolutions, the surface of especially the big bubbles cannot be reconstructed quantitatively, due to reflections, glare points and shadows of waves on the bubbles surfaces.

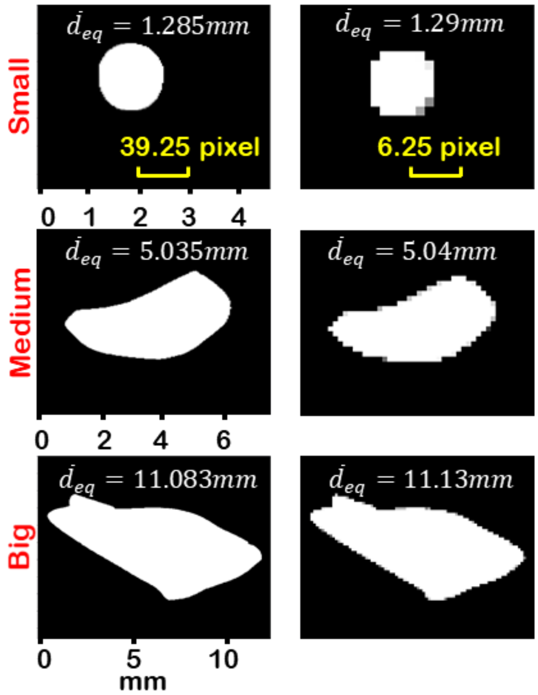

Figure 4. Comparison of original resolution for the 3D-reconstruction of small, medium and big bubbles.

3.3. Computing costs

Measurements performed with high resolution often come under premises of very high computing costs. In the following tables, the computing time on an Intel Core I9-9940X, 14 cores@4.4 GHz with 64 GB RAM and the final file size of an exported DAT-file and the DaVis intern VC7-file are listed for different resolutions of the Tomographic Sizing Reconstruction of bubbles (Table 1) and the Fine Scale Reconstruction of a STB flow field (Table 2). The finest resolution (6 voxel grid) of the FSR VIC# was calculated on the CPU and GPU (NVIDIA Quadro P400, 2 GB). The computing steps of the STB, the calculation of the trajectories and other image processing steps are relatively fast compared to the Tomographic Sizing Reconstruction of the bubbles and the FSR VIC# and are therefore not taken into account.

The final file sizes are especially a problem when trying to merge the different data types together. Humongous DAT-Files (ASCII) are not easy to handle since they overflow most of common editors, like MatLab, NotePad++ or PilotEdit. But even the calculation of the trajectories from reconstructed bubbles becomes a challenge, because the high resolution images have to be reloaded for the calculation, requiring very high RAM, which is the reason why only low resolution reconstructions (Figure 4) were used for the calculation of the trajectories as shown in section 4.

Table 1: Computing time of 250 time steps/images for the 3D bubble reconstruction, file size (.dat/.vc7) of one time step

Resolution	Time	File Size	Reconstructed Volume
6.25 pixel/mm	5 min	592/75 MB	314 x 439 x 189 voxels
12.5 pixel/mm	32 min	4.7/0.59 GB	626 x 879 x 376 voxels
25 pixel/mm	3.6 h	(36.8)/4.6 GB	1251 x 1751 x 751 voxels
39.25 pixel/mm	11.5 h	(46.3)/5.8 GB	1964 x 2749 x 1179 voxels

Table 2: Computing time of 250 time steps/images for the Fine Scale Reconstrucion VIC#, file size (.dat/.vc7) of one time step.

Grid resolution	Time	File Size	Reconstructed Volume
24 voxel	6 h	55/10 MB	82x113x33 vectors
16 voxel	20 h	185/28 MB	123x169x50 vectors
12 voxel	36 h	324/76 MB	164x226x66 vectors
6 voxel	412 h (+GPU)	2.7/0.6 GB	328x451x131 vectors

4. RESULTS

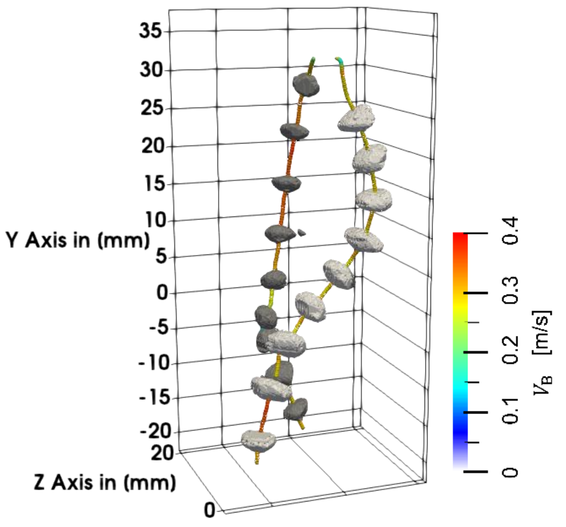

Figure 5. Trajectories of two bubbles (dark and light grey) bouncing on each other in a bubble swarm; Trajectories show the local velocity of the bubbles; time step between the depicted bubbles Δt = 20 ms.

Figure 5 shows the trajectories of two colliding bubbles. Due to the reconstruction method, the trajectories of each individual bubble end, as soon as the bubbles are so close to each other that their shadow image is merging in the processing. Therefore, the resulting trajectory for these time steps was calculated by the mass centre of both bubbles, even though they are not merging in reality. However, the trajectories before and after the collision visualize the bubble velocities of each bubble and the energy conversion between the bubbles after the collision very precisely. The smaller and slower bubble (dark grey) is oscillating after the collision and becomes then faster than the bigger bubble (light grey), which was faster before the collision.

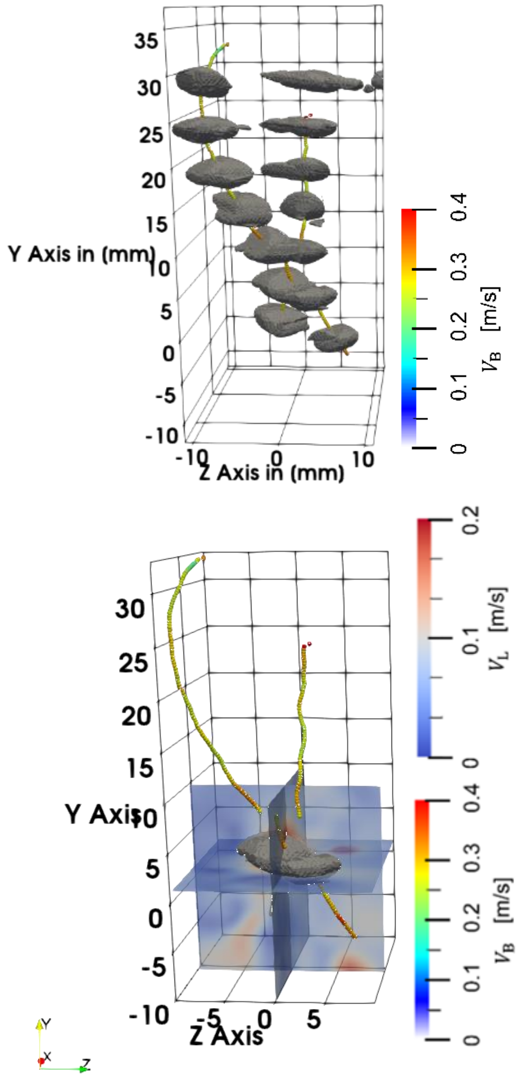

Figure 6. Top: Trajectories of two bubbles (grey) bouncing on each other in a bubble swarm; Trajectories show the local velocity of the bubbles, time step between the depicted bubbles Δt = 20 ms; Bottom: planes show the local liquid velocity field at the moment of collision t = 20 ms.

Figure 6 shows the combination of the trajectories and reconstructed bubbles (top), so the bubble motion, and the volumetric flow field around the bubbles (bottom).

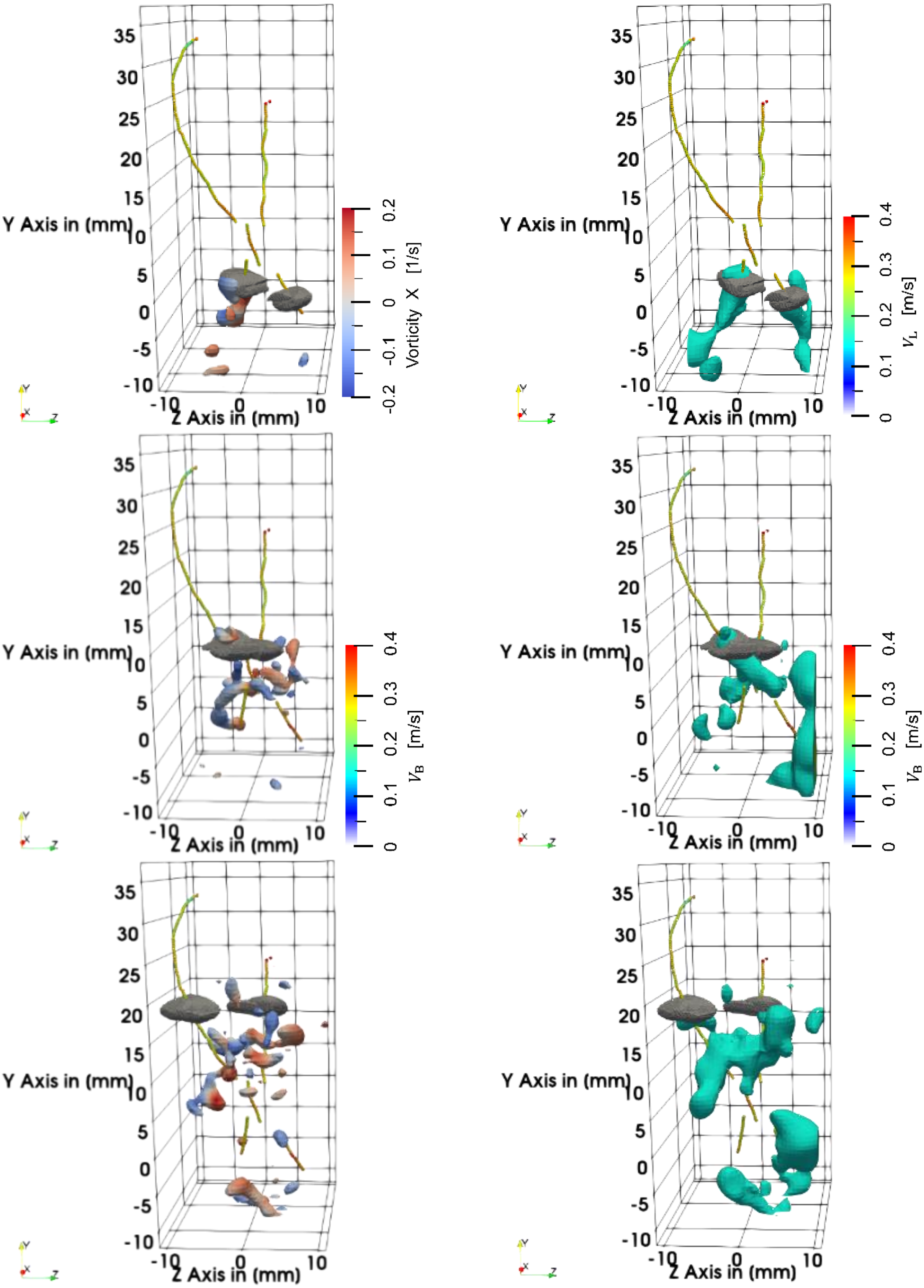

Figure 7. Two bubbles (grey) colliding, trajectories show the average bubble velocity; left column: isosurface of Q-criterion = 0.0035…0.03 coloured with vorticity in x-direction; right column: isosurface of velocity v_L = 0.15 m/s, time step $\Delta t = 40ms$.

Because it is difficult to visualize lots of different three dimensional and time-resolved data in one image, in Figure 7 three time steps of the collision of Figure 6 are shown on different images. The isosurface of the Q-criterion (Q = 0.0035…0.03), visualizes the vortex occurrence coloured with the vorticity in x-direction (left column), and an isosurface of constant velocity (v_L = 0.15 m/s) visualizes the main flow direction (right column).

The following Figure 8 shows the bubble swarm as isosurface (grey) after 100 ms. The bubble's trajectories visualise the bubble velocity and the planes (YX and YZ) show the liquid flow field around the bubbles as vector field (3000 vectors equidistant over boundaries).

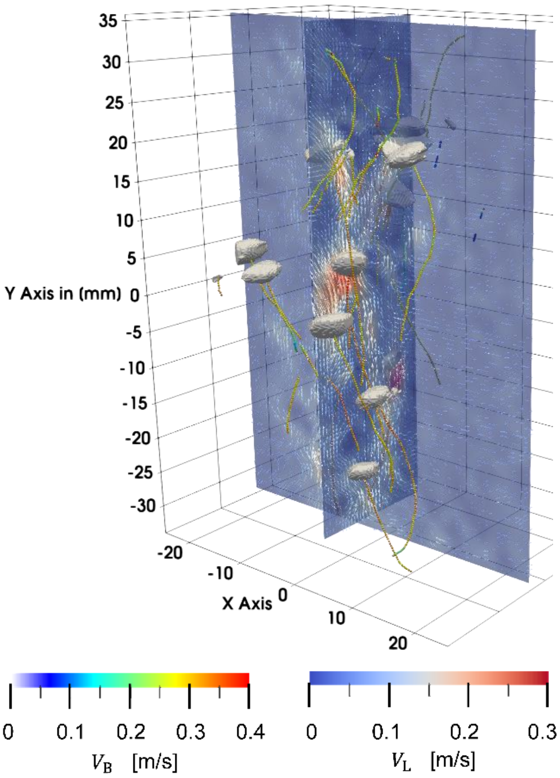

Figure 8. Bubble swarm at time step *t* = 100 ms (grey) with trajectories (bubble velocity) and liquid velocity vector field in YX and YZ plane.

In both figures (Figure 7 and 8), the flow field around the bubbles shows a physical behaviour. The bubble velocities, the flow field and vortex structures are in a good agreement. However, the local resolution close to the bubble surface needs further improvement, because vectors for the liquid phase are interpolated into the bubbles. Therefore, a higher particle density and an improved postprocessing are mandatory. The reconstructed bubbles should be used as masking functions, creating a physical phase boundary. This would enable a more realistic flow field reconstruction close to the bubbles and a good visualization of streamlines.

5. CONCLUSION

The goal of this work was to evaluate an experimental set-up for the simultaneous characterization of the flow field around bubbles in a bubble swarm and the bubble's shape, size and trajectories. Therefore, a high-speed tomographic shadowgraphy system with four cameras and a triggered LED volume illumination was implemented. Thanks to the STB algorithm high resolution flow fields around each bubble could be reconstructed, even though a higher particle concentration of 0.125 ppp is preferable, but was not feasible in our case, due to the relatively big column volume.

The overall camera setup delivers good results under the assumption that the flow around a bubble is symmetrical, since all cameras are set on one side of the bubble column. A setup with 6 cameras or more around the tank could deliver more precise data, since tracer particles cannot disappear behind bubbles and bubbles in a swarm are not overlapping each other so much in the camera views.

In the future the reconstructed bubbles from the tomographic sizing process should be used as geometric mask and be implemented into the Fine Scale Reconstruction process after the STB reconstruction. This mask can then assure a better reconstruction of the flow field around the bubbles and a detailed analysis of the streamlines. This bubble surface could be set as a wall function with parameters of the bubble motion and its velocity, which would further improve the physics of the reconstruction model, since liquid is being displaced by the bubbles and does not flow through it. The interaction between bubbles in a bubble swarm, the behaviour when bubbles collide, and the influence of the bubbles wake can then be measured in very high resolution as shown in Figure 8.

The reconstruction of the bubble surface stays a complicated task, due to light reflections and glare points. Especially the surface of big bubbles often shows waves, indents and other inconsistent structures messing with the segmentation process. The method is certainly not applicable to realistic bubble column gas fractions, but can help to understand single bubble behaviour, evaluate models and numerical simulations. The afore presented measurements are only a first step to this end and many experience will be necessary to allow for the acquisition of spatially and temporally resolved reliable data sets.

REFERENCES

[1] Aoyama, S.; Hayashi, K.; Hosokawa S.; Tomiyama, A.; 2018; "Shapes of single bubbles in infinite stagnant liquids contaminated with surfactant" *Exp Therm Fluid Sci* 96:460-469 doi: 10.1016/j.expthermflusci.2018.03.015

[2] Filella, A.; Ern, P.; Roig, V; 2015; "Oscillatory motion and wake of a bubble rising in a thin-gap cell"; *Journal of Fluid Mechanics; 778*, 60-88; doi:10.1017/jfm.2015.355

[3] Mikaelian, D.; Larcy, A.; Dhaeck, S.; Haut, B.; 2013; "A new experimental method to analyse the dynamics and the morphology of bubbles in liquids: Application to single ellipsoidal bubbles"; *Chemical Engineering Science*, 100, 529-538; http://dx.doi.org/10.1016/j.ces.2013.04.013

[4] Hassan, Y. A.; Oritz-Villafuerte, J.; Schmidl, W. D.; 2000; "Three-dimensional measurements of single bubble dynamics in a small diameter pipe using stereoscopic particle image velocimetry"; *International Journal of Multiphase Flow* 27 817-842

[5] Liu, Z.; Zheng, Y.; 2006; "PIV study of bubble rising behaviour"; *Powder Technology* 168 10-20; doi:10.1016/j.powtec.2006.05.020

[6] Yoshimoto, K.; Saito, T.; 2010; "3-dimensional liquid motion around a zigzagging ascent bubble measured using tomographic Stereo PIV"; *15th Int Symp on Applications of Laser Techniques to Fluid Mechanics*

[7] Schanz, D.; Gesemann, S.; Schröder, A.; 2016; "Shake-The-Box: Lagrangian particle tracking at high particle image densities"; *Experiments in Fluids*. 57; doi: 10.1007/s00348-016-2157-1.

[8] Schneiders, J.; Scarano, F.; 2016; "Dense velocity reconstruction from tomographic PTV with material derivatives" *Experiments in Fluids*: *experimental methods and their applications to fluid flow*, 57, [139]. https://doi.org/10.1007/s00348-016-2225-6

[9] Sellappan, P.; Alvi, F. S.; Cattafesta, L. N.; 2020, "Lagrangian and Eulerian measurements in high-speed jets using Multi-Pulse Shake-The-Box and fine scale reconstruction (VIC#)" *Experiments in Fluids* 61:157; https://doi.org/10.1007/s00348-020-02993-9

[10] Lee, J.; Park, H.; 2022; "Flow induced by the single-bubble chain depending on the bubble release frequency"; *Physics of Fluids 34, 033312 (2022);* https://doi.org/10.1063/5.0083281

[11] She, W.; Gao, Q.; Zuo, Z.; Liao, X.; Zhao, L.; Zhang, L.; Nie, D.; Shao, X.; 2021; "Experimental study on a zigzagging bubble using tomographic particle image velocimetry with shadow image reconstruction"; *Physics of Fluids 33, 083313(2021);* doi:10.1063/5.0057198

[12] Zhang, J.; Ni, M.; Magnaudet, J.; 2021; "Three-dimensional dynamics of a pair of deformable bubbles rising initially in line. Part 1. Moderately inertial regimes"; *Journal of Fluid Mechanics, Cambridge University Press (CUP);* 320, pp.A16. 10.1017/jfm.2021.429. hal-03382547; https://doi.org/10.1017/jfm.2021.429

[13] Zhang, J.; Ni, M.; Magnaudet, J.; 2021; "Three-dimensional dynamics of a pair of deformable bubbles rising initially in line. Part 2. Highly inertial regimes"; *Journal of Fluid Mechanics, Cambridge University Press (CUP);* https://arxiv.org/abs/2201.09336v1

[14] Jeon, Y. J.; Müller, M., Michaelis, D.; Wieneke, B.; 2019; "Data assimilation-based flow field reconstruction from particle tracks over multiple time steps"; *13th International Symposium on Particle Image Velocimetry – ISPIV 2019*

[15] Raffel, M.; Willert, C. E.; Scarana, F.; Kähler, C. J.; Wereley, S. T.; Kompenhans J.; "Particle Image Velocimetry, A Practical Guide" Third Edition; Springer-Verlag Berlin Heidelberg; ISBN 978-3-319-+9962-0; https://doi.org/10.1007/978-3-319-68852-7